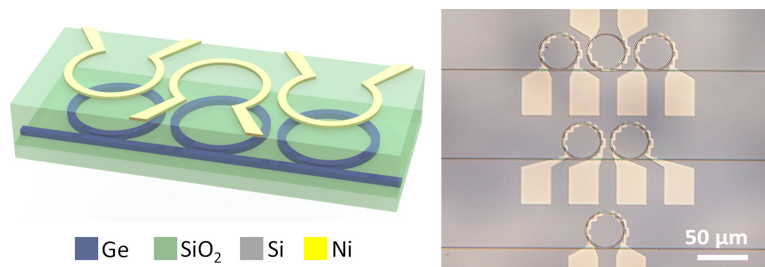# Tunable Germanium-on-Insulator Band-Stop Optical Filter Using Thermo-Optic Effect

Chong Pei Ho
Ziqiang Zhao
Qiang Li
Shinichi Takagi
Mitsuru Takenaka

Ge SiO$_2$ Si Ni

50 μm

Tunable Germanium-on-Insulator Band-Stop Optical Filter Using Thermo-Optic Effect

Chong Pei Ho [ORCID]**, Ziqiang Zhao** [ORCID]**, Qiang Li** [ORCID]**, Shinichi Takagi, and Mitsuru Takenaka** [ORCID]

The authors are with the Department of Electrical Engineering and Information Systems,
The University of Tokyo, Tokyo 113-8656, Japan

Abstract: We demonstrate a tunable band-stop optical filter on a germanium-on-insulator photonic platform operating at 1.95 μm wavelength. The band-stop filter is implemented using parallel-coupled microring resonators with the number of microring resonators varied from one to. three. Through the use of a heating stage, the thermo-optic coefficient of germanium is measured to be $+3.55 \times 10^{-4}$/°C. The high thermo-optic coefficient of germanium is exploited by including metal heating lines to provide localized on-chip tuning. As predicted by theoretical analysis, our experimental results show that when the number of microring resonators increases, the -3 dB bandwidth and extinction ratio of the optical filter increases. With the number of microring resonators increases from one to three, the -3 dB bandwidth of the filter increases from 0.283 to 0.661 nm and the extinction ratio from 9.56 to 22.10 dB.

Index Terms: Tunable filter, optical resonators, thermal effects.

1. Introduction

As the desire for more global data traffic and communication bandwidth increase exponentially in recent years, much interest has been directed towards photonics as the platform for the realization of "More than Moore" micro/nano-systems [1], [2]. In particular, in order to extend beyond the telecommunication wavelengths, recent research interests have been concentrated around mid-infrared (MIR) photonics. Germanium (Ge) has recently emerged as an ideal optical material for MIR photonics due to its large transparency window in the MIR wavelengths as well as the possibility of integration with lasing and light detection devices based on strained Ge and germanium tin (GeSn) material constellation [3]–[5]. Ge also has higher refractive index of around 4.1 and around ten times larger Kerr coefficient than Si [6]. For tuning of the photonic performance through thermo-optic effect, Ge also proves to be a more superior material choice for its higher thermo-optic coefficient than Si [6], [7].

An optical filter, in the form of a band-stop filter, is an essential component for any photonic communication network in order to remove an unwanted channel from multiplexed channel outputs. One of the more promising design architectures for such band-stop filter is the use of parallel-
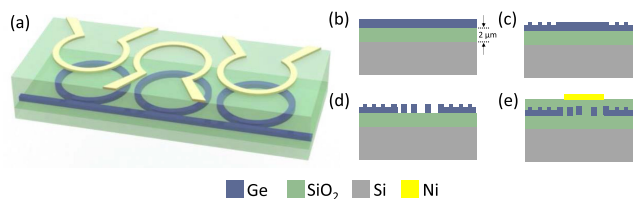
Fig. 1. (a) Schematic of the tunable GeOI band-stop filter with heater lines and (b)–(e) fabrication process of GeOI band-stop filter.

coupled microring resonators where the −3 dB bandwidth and the extinction ratio is dependent on the number of cascaded microring resonators [8]–[10]. However, in view of fabrication variations, it is often difficult to achieve identical microring resonators [11]. In order to overcome this, the usage of an overlaying heater to induce thermo-optic tuning is often deployed [12]–[14]. Due to the much higher thermo-optic coefficient of Ge, such tuning proves to be more efficient and hence power-saving. In order to fully harness the optical advantages of Ge, we have previously realized high quality germanium-on-insulator (GeOI) photonic platform [6]. Compared to other Ge photonic platforms such as Ge-on-silicon (GOS) and Ge-on-silicon-on-insulator (SOI), GeOI offers better optical confinement due to higher refractive index contrast [15]. More importantly, thermo-optic tuning on both GOS and Ge-on-SOI photonic platforms face the problem of heat retention and hence higher power consumption. As the thermal conductivity of silicon (Si) is relatively high at 130 Wm^{-1}K^{-1} [16], the underlying Si layer effectively acts as a heat sink, hence preventing any efficient heating on the Ge photonic patterns. In order to prevent such heat loss, undercutting the Si for GOS or silicon dioxide (SiO$_2$) for Ge-on-SOI is utilized which vastly complicates the fabrication process [17], [18].

In this study, a tunable band-stop filter is implemented on a GeOI photonic platform. By using various numbers of parallel-coupled microring resonators, the −3 dB bandwidth and extinction ratio can be controlled. As mentioned above, when the number of microring resonators increases, fabrication variations cause the resonance wavelengths of the various microring resonators to differ slightly. To overcome this, Ni metal lines are used to induce thermo-optic effect through joule heating. As the thermo-optic coefficient of Ge is much higher than Si, it is expected that lower power is required [19]. At the same time, such thermo-optical tuning is typically able to provide a tuning speed in the range of 0.1 ms [20]–[24]. When the number of microring resonators increases from one to three, it is observed that the −3 dB bandwidth increases from 0.377 nm to 0.661 nm and the extinction ratio increases from 12.249 dB to 22.098 dB.

2. Device Design and Fabrication

Fig. 1(a) shows the schematic of the tunable GeOI band-stop filter. In order to ensure single mode operation, the thickness of the Ge layer is controlled to be around 240 nm and the waveguide is designed to be 500 nm. The radius of the microring resonator is 20 μm and the gap from the waveguide is 100 nm. A nickel (Ni) metal line of 3 μm wide and 120 nm thick is implemented on each microring resonator to provide localized tuning. The distance between adjacent microring resonators is 50 μm so as to achieve optical and thermal isolation.

Fabrication of the device begins with previously demonstrated Smart-cut process to produce the GeOI wafer as shown in Fig. 1(b) [6], [25], [26]. An electron beam lithography (EBL) and deep reactive ion etching (DRIE) are first performed to define the grating couplers which includes a half-etch of the Ge layer as depicted in (c). A subsequent EBL and DRIE are done to define the microring resonators and waveguides, as shown in (d). The structures are then cladded using 1-μm-thick SiO$_2$ using plasma-enhanced chemical vapor deposition (PECVD). Finally, as shown in (e), Ni metal lines are sputtered and defined using lift-off process. The scanning electron microscope (SEM) image of the fabricated single microring resonator structure is shown in Fig. 2(a). The microscope image of
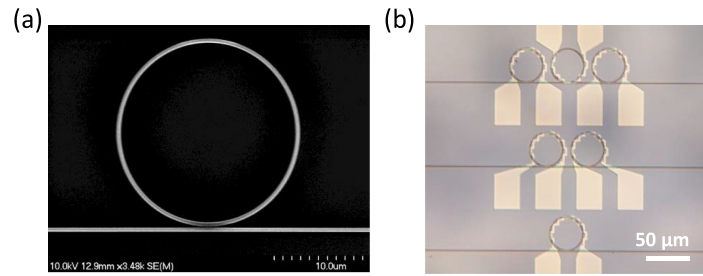
(a)   (b)

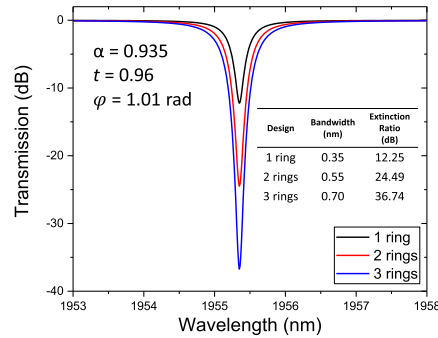Fig. 2. (a) SEM image and (b) microscope image of the fabricated devices.

Fig. 3. Theoretical analysis of the band-stop filter with one to three microring resonators.

the fabricated devices with one to three microring resonators is shown in (b). A corrugated design is used for the Ni heater lines to increase the resistance and better heat concentration above the microring resonator designs.

3. Modelling and Experimental Results

A combination of finite-difference time-domain (FDTD) and theoretical analysis are used to simulate the performance of the band-stop filter. A theoretical approach is adopted in order to avoid the large computation resource needed for FDTD simulations when multiple ring resonators are used. Using FDTD simulation, the performance of a single microring resonator is first simulated. The simulated Q-factor is around 8000 and the extinction ratio is 12.44 dB. A calculative analysis is then implemented to match the resonance. The loss coefficient of the ring, α, is 0.935. The output power, P_t, of the microring resonator can be calculated using

$$P_t = |E_t|^2 = \frac{\alpha^2 + |t|^2 - 2\alpha\,|t|\cos(\theta + \varphi)}{1 + \alpha^2|t|^2 - 2\alpha\,|t|\cos(\theta + \varphi)}$$

where $t = |t|\exp(j\varphi)$ and $\theta = \beta L$ is the single pass phase shift, with L the round-trip length and β the propagation constant of the circulating mode. $|t|$ and φ represent the coupling losses and phase of the coupler between the microring resonator and waveguide and are set to 0.96 and 1.01 rad respectively. The transmitted power is 0 on the critical coupling condition that $|t|$ is equal to α [27]. Using these parameters, the performance of the band-stop filter using one to three rings are shown in Fig. 3. As depicted, the bandwidth and extinction ratio of the band-stop filter increases from 0.35 nm to 0.70 nm and 12.25 dB to 36.74 dB when the number of microring resonators increases from one to three.

The thermo-optic coefficient of Ge is first experimentally investigated by varying the temperature of the sample stage from 20°C to 30°C. The resonance of a single microring resonator is found to have redshift by 0.179 nm/°C, as shown in Fig. 4(a). The corresponding thermo-optic coefficient
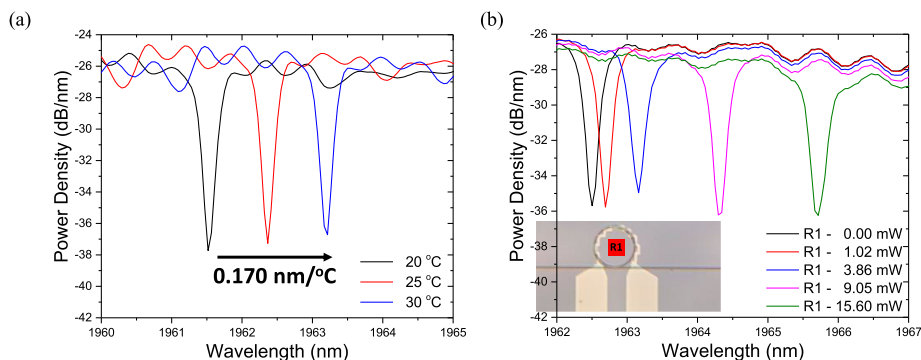
Fig. 4. Measurement of a single microring resonator by (a) changing the temperature of sample stage and (b) using various power on the Ni metal line.
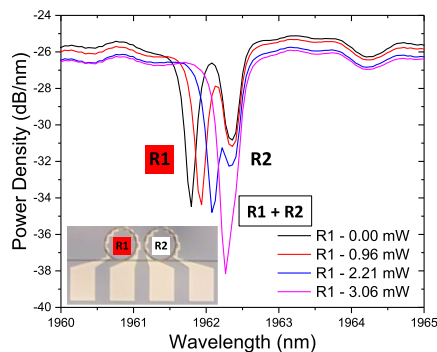

Fig. 5. Measurement of the band-stop filter with two microring resonators using various power on the Ni metal line on R1.

of Ge can hence be calculated to be $+3.55 \times 10^{-4}$ /°C, which is more than twice of Si which is $+1.60 \times 10^{-4}$ /°C. Similarly, by applying current through the Ni metal lines, localized joule heating of the microring resonator can also be achieved. The resistance of the Ni metal line is measured to be around 0.99 kΩ. The measurement of a single microring resonator using the Ni metal line heater is shown in Fig. 4(b). As shown, the resonance wavelength of the microring resonator follows a redshift as the power in the metal line increases. When the power through the metal line is 15.60 mW, the resonance wavelength shifts by 3.159 nm. After removing the coupling efficiency of the grating couplers used, the insertion loss of the filter is also estimated to be around 5 dB.

As the number of microring resonators increases, it was found that numerous resonances are observed. This is due to fabrication and thickness variation across the device. Fig. 5 shows the measurement result of the band-stop filter with two microring resonators. Due to the abovementioned variations, it is found that the resonance of R1 is at a slightly lower wavelength than the resonance of R2. In order to overcome this, the Ni metal line on R1 is used to tune the resonances to a single wavelength. As power is applied on R1, the resonance of R1 redshifts as expected while the resonance due to R2 is remains stationary. When a power of 3.06 mW is applied on R1, the resonances of the two microring resonators combine at 1962.267 nm, resulting in a boarder band-stop bandwidth and higher extinction ratio.

When the number of microring resonator increases to three, similar phenomenon of numerous resonances is also observed, as shown in Fig. 6(a). It is noted that R1 displays a slight resonance-splitting which can be attributed to the rough sidewalls induced in the fabrication. This causes the presence of propagating and counter-propagating modes in R1 which interact and result in a split resonance [28], [29]. When R1 is tuned at a power of 9.05 mW, the resonance of R1 combines with the resonance of R3. An identical approach is used to tune the resonance of R2 to combine with
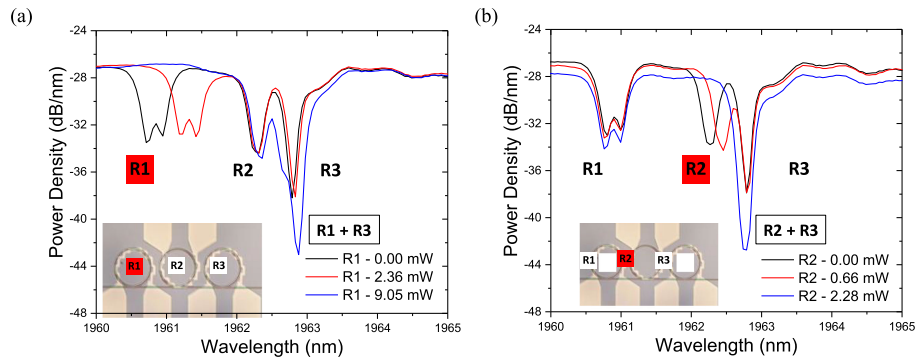
Fig. 6. Measurements of the band-stop filter with three microring resonators (a) using various power on the Ni metal line on R1 and (b) R2.
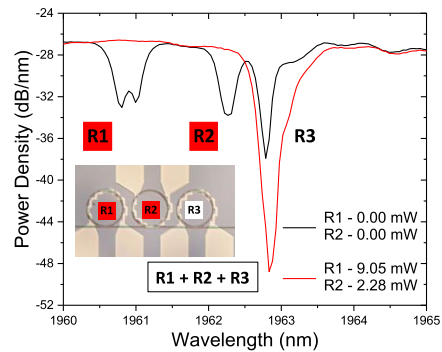

Fig. 7. Measurement of the band-stop filter with three microring resonators when power is applied to both R1 and R2.
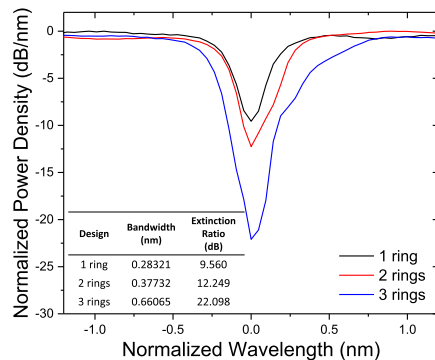

Fig. 8. Summary of results of band-stop filter with different number of microring resonators.

the resonance of R3 as shown in (b). In this case, a power of 2.28 mW is required. As depicted in Fig. 7, when the appropriate powers are applied to R1 and R2 simultaneously, the resonances of the three microring resonators are tuned to a single wavelength of 1962.833 nm.

The measurement results of the band-stop filters are summarized in Fig. 8. Both the power density and wavelengths are normalized for easier comparison across the different designs. As predicted by theoretical analysis, when the number of microring resonators increases, the bandwidth of the band-stop filter increases. When there is one microring resonator, the 3 dB bandwidth is 0.283 nm and it increases to 0.378 nm and 0.661 nm when the number of microring resonators increases to two and three respectively. The extinction ratio of the band-stop filter also displays similar trend
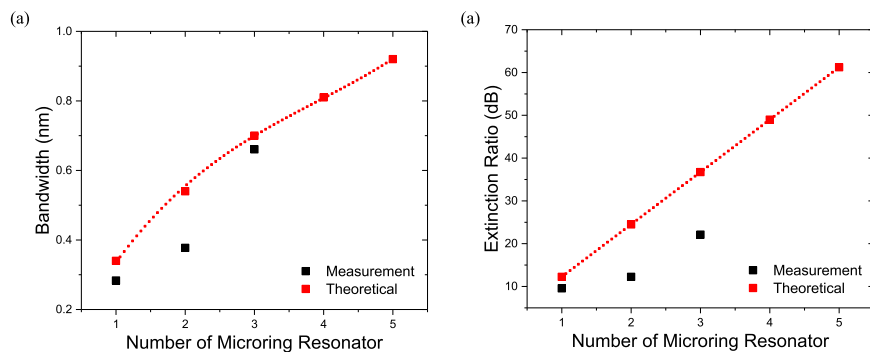
Fig. 9. Comparison of the measured and theoretical (a) bandwidth and (b) extinction ratio with various number of microring resonators.

when it increases from 9.560 dB in a single microring resonator design to 11.830 dB when there are two microring resonators. When three microring resonators are utilized, the extinction ratio is 22.098 dB. Higher extinction ratio is not obtained due to the measurement limit of the optical spectrum analyzer that is used in the setup.

The measurement results of the band-stop filters are compared with theoretical analysis as depicted in Fig. 9. As shown from the theoretical analysis in (a), when the number of microring resonator increases, the bandwidth of the band-stop filter increases as well. This is also true for the extinction ratio which escalates linearly with the number of microring resonator as presented in (b). Although the measurement results deviate from the theoretical analysis due to significant fabrication variations, the increasing trends are present in both cases. Based on the need and requirement of the application, the proposed band-stop filter can be utilized with an appropriate number of microring resonators [30]–[32]. As shown experimentally, the thermo-optic coefficient of GeOI is around $+3.55 \times 10^{-4}$ /°C, which is more than twice of Si. By harnessing the enhanced thermo-optic coefficient of the GeOI platform, a more efficient thermal tuning can be realized. As thermo-optic coefficient is a material property, this indicates that GeOI is a good candidate to overcome the limitations faced by SOI platform.

4. Conclusion

In conclusion, we have demonstrated a tunable band-stop filter which is implemented on a GeOI photonic platform. By using various numbers of parallel-coupled microring resonators, the −3 dB bandwidth and extinction ratio of the band-stop wavelengths can be controlled. When only one microring resonator is used, the device displays a bandwidth of 0.283 nm and an extinction ratio of 9.560 dB. When increasing the number of microring resonators, numerous resonances are observed due to fabrication and thickness variations. In order to overcome this, Ni metal lines are used to induce thermo-optic effect through joule heating. Due to the high thermo-optic coefficient of Ge of $+3.55 \times 10^{-4}$ /°C, it is expected that lower power is required. It is also noted that adjacent microring resonators are thermally isolated and are not affected by the heating. By utilizing this scheme, the resonances of various microring resonators are tuned at an efficiency of 0.203 nm/mW to a single wavelength. When two microring resonators are used, the −3 dB and extinction ratio measured are 0.377 nm and 12.249 dB. The −3 dB and extinction ratio increase to 0.661 nm and 22.098 dB when three microring resonators are implemented. This shows the feasibility of using such tunable GeOI band-stop filter for future realization in communication systems.

Acknowledgment

References

[1] W. Bogaerts *et al.*, "Nanophotonic waveguides in silicon-on-insulator fabricated with CMOS technology," *J. Lightw. Technol.*, vol. 23, no. 1, pp. 401–412, Jan. 2005.

[2] A. Ghiasi, "Large data centers interconnect bottlenecks," *Opt. Exp.*, vol. 23, pp. 2085–2090, 2015.

[3] J. R. Sánchez-Pérez *et al.*, "Direct-bandgap light-emitting germanium in tensilely strained nanomembranes," *Proc. Nat. Acad. Sci.*, vol. 108, pp. 18893–18898, 2011.

[4] U. Younis *et al.*, "Towards low-loss waveguides in SOI and Ge-on-SOI for mid-IR sensing," *J. Phys. Commun.*, vol. 2, 2018, Art. no. 045029.

[5] Y.-H. Peng, H. Cheng, V. I. Mashanov, and G.-E. Chang, "GeSn pin waveguide photodetectors on silicon substrates," *Appl. Phys. Lett.*, vol. 105, 2014, Art. no. 231109.

[6] J. Kang, M. Takenaka, and S. Takagi, "Novel Ge waveguide platform on Ge-on-insulator wafer for mid-infrared photonic integrated circuits," *Opt. Exp.*, vol. 24, pp. 11855–11864, 2016.

[7] C. P. Ho *et al.*, "Characterization of polycrystalline silicon-based photonic crystal-suspended membrane for high temperature applications," *J. Nanophoton.*, vol. 8, 2014, Art. no. 084096.

[8] J. Cardenas *et al.*, "Wide-bandwidth continuously tunable optical delay line using silicon microring resonators," *Opt. Exp.*, vol. 18, pp. 26525–26534, 2010.

[9] Y. Hu *et al.*, "An ultra-high-speed photonic temporal differentiator using cascaded SOI microring resonators," *J. Opt.*, vol. 14, 2012, Art. no. 065501.

[10] Y. Hu *et al.*, "High-speed silicon modulator based on cascaded microring resonators," *Opt. Exp.*, vol. 20, pp. 15079–15085, 2012.

[11] P. Dong, A. Melikyan, and K. Kim, "Commercializing silicon microring resonators: Technical challenges and potential solutions," in *Proc. Conf. Laser Eletro Opt.*, 2018, vol. 3, Paper SM4B.

[12] H.-T. Kim and M. Yu, "High-speed optical sensor interrogator with a silicon-ring-resonator-based thermally tunable filter," *Opt. Lett.*, vol. 42, pp. 1305–1308, 2017.

[13] H. Xiao *et al.*, "Tunable Fano resonance in mutually coupled micro-ring resonators," *Appl. Phy. Lett.*, vol. 111, 2017, Art. no. 091901.

[14] S. Gan *et al.*, "A highly efficient thermo-optic microring modulator assisted by graphene," *Nanoscale*, vol. 7, pp. 20249–20255, 2015.

[15] S. Kim, J.-H. Han, J. P. Shim, H. J. Kim, and W. J. Choi, "Verification of Ge-on-insulator structure for a mid-infrared photonics platform," *Opt. Mater. Exp.*, vol. 8, no. 2, pp. 440–451, 2018.

[16] W. Liu and M. Asheghi, "Thermal conductivity measurements of ultra-thin single crystal silicon layers," *J. Heat Transfer*, vol. 128, pp. 75–83, 2006.

[17] A. Malik *et al.*, "Ge-on-Si and Ge-on-SOI thermo-optic phase shifters for the mid-infrared," *Opt. Exp.*, vol. 22, pp. 28479–28488, 2014.

[18] S. Radosavljevic *et al.*, "Mid-infrared Vernier racetrack resonator tunable filter implemented on a germanium on SOI waveguide platform," *Opt. Mater. Exp.*, vol. 8, no. 4, pp. 824–835, 2018.

[19] T. Fujigaki, S. Takagi, and M. Takenaka, "High-efficiency Ge thermo-optic phase shifter on Ge-on-insulator platform," *Opt. Exp.*, vol. 27, no. 5, pp. 6451–6458, 2019.

[20] M. Geng *et al.*, "Four-channel reconfigurable optical add-drop multiplexer based on photonic wire waveguide," *Opt. Exp.*, vol. 17, no. 7, pp. 5502–5516, 2009.

[21] P. Dong *et al.*, "Thermally tunable silicon racetrack resonators with ultralow tuning power," *Opt. Exp.*, vol. 18, no. 19, pp. 20298–20304, 2010.

[22] H. T. Kim and M. Yu, "High-speed optical sensor interrogator with a silicon-ring-resonator-based thermally tunable filter," *Opt. Lett.*, vol. 42, no. 7, pp. 1305–1308, 2017.

[23] S. Chen *et al.*, "A 45 nm CMOS-SOI monolithic photonics platform with bit-statistics-based resonant microring thermal tuning," *IEEE J. Solid-State Circuits*, vol. 51, no. 4, pp. 893–907, Apr. 2016.

[24] K. Chen, F. Duan, and Y. Yu, "High-performance thermo-optic tunable grating filters based on laterally supported suspended silicon ridge waveguide," *Opt. Exp.*, vol. 26, no. 15, pp. 19479–19488, 2018.

[25] J. Kang, X. Yu, M. Takenaka, and S. Takagi, "Impact of thermal annealing on Ge-on-Insulator substrate fabricated by wafer bonding," *Mater. Sci. Semicond. Process.*, vol. 42, pp. 259–263, 2016.

[26] T. H. Xiao *et al.*, "High-Q germanium optical nanocavity," *Photon. Res.*, vol. 6, no. 9, pp. 925–928, 2018.

[27] R. G. Dominik, "Ring resonators: Theory and modeling," *Integr. Ring Resonators*, vol. 127, pp. 3–40, 2007.

[28] Q. Li, Z. Zhang, J. Wang, M. Qiu, and Y. Su, "Fast light in silicon ring resonator with resonance-splitting," *Opt. Exp.*, vol. 17, pp. 933–940, 2009.

[29] Q. Li, T. Wang, Y. Su, M. Yan, and M. Qiu, "Coupled mode theory analysis of mode-splitting in coupled cavity system," *Opt. Exp.*, vol. 18, pp. 8367–8382, 2010.

[30] R. K. Sinha, M. Wan, S. K. Bag, and S. K. Varshney, "Design and fabrication of microring resonator array for mid-IR filter applications," *Frontiers Opt.*, 2018, Paper JTu3A-19.

[31] H. Xiao *et al.*, "Experimental realization of a CMOS-compatible optical directed priority encoder using cascaded micro-ring resonators," *Nanophotonics*, vol. 7, no. 4, pp. 727–733, 2018.

[32] H. J. Caulfield and S. Dolev, "Why future supercomputing requires optics," *Nature Photon.*, vol. 4, no. 5, p. 261, 2010.